ELSEVIER

Journal of Wind Engineering
and Industrial Aerodynamics 67&68 (1997) 195–208

JOURNAL OF wind engineering AND industrial aerodynamics

Numerical simulation of flow around rectangular prism

Da-hai Yu*, Ashan Kareem

Department of Civil Engineering and Geological Science, University of Notre Dame, Notre Dame, IN 46556, USA

Abstract

Using the large eddy simulation (LES), both two-dimensional (2D) and three-dimensional (3D) simulations of the velocity and pressure fields surrounding a rigid rectangular prism at a Reynolds number of 10^5 are conducted. A finite difference numerical scheme based on a staggered grid is employed. The convection terms are discretized with either QUICK or central difference schemes, while the Leith method is employed for temporal marching. The computed mean velocity along the symmetry line is compared with experimental results as well as numerical results reported by other investigators. It is in closer agreement with the experimental results than other reported numerical results. The mean, the root mean square (RMS) pressure distribution on the prism surface, and the integral forces (lift and drag) are computed. The correlation coefficients of pressure at different chordwise locations around a square prism are also calculated. These simulations are found to be in very good agreement with available experimental results reported in the literature. Both QUICK and central difference schemes are used to discretize the convection terms, and the upwinding effect of the QUICK scheme is investigated. A grid refinement study is also conducted to evaluate the effects of grid size on the simulation results.

Keywords: Large eddy simulation; Turbulence; Bluff-body flow

1. Introduction

With developments in computational fluid dynamics and the ever-growing capabilities of computers, numerical methods are becoming a promising analysis tool in the modeling of wind-structure interactions. Turbulence models are developed to simulate high Reynolds number flows that are not achievable with direct numerical simulation due to computer limitations. Literature suggests that the large eddy

* Corresponding author. E-mail: dyul@darwin.cc.nd.edu.

PII S0167-6105(97)00073-1

simulation (LES) scheme is more attractive due to its higher accuracy in comparison with techniques based on Reynolds-averaged Navier–Stokes equations. In LES, fluid motions at scales larger than a prescribed filter size are resolved and solved directly, while smaller scales are modeled by a subgrid-scale (SGS) model.

Murakami and his group conducted a series of numerical studies involving two-dimensional square cylinders [1]. Their study has shown that the 3D modeling provides a better representation of the flow characteristics than the 2D case, and the LES modeling provides a better and more realistic simulation of the flow field. Tamura [2] simulated the flow field around a square prism using the dynamic SGS model. He also conducted the same simulation by employing a third-order upwind scheme to discretize the convection terms without a SGS model. He concluded that average and root mean square (RMS) values can be predicted by the computation with reasonable grids, while other statistics, like the correlation of unsteady pressures, did not compare well with the experimental data despite a large number of grid points (4 million). To assess the current state of the art in LES for flow past bluff bodies, a workshop was held in Germany in 1995 [3], where employed methods and obtained results provided by a number of contributors were compared. Besides the numerical simulations, a number of experimental studies are available in the literature. They can be used as a data base for validating numerical results.

2. Governing equations and numerical methods

The Navier–Stokes equations for an incompressible fluid, combined with a subgrid-scale turbulence model, are used herein in LES of the flow around a rectangular prism. In this study, the Smagorinsky model is used for the subgrid-scale viscosity

$$\frac{\partial \bar{u}_i}{\partial t} + \bar{u}_j \frac{\partial \bar{u}_i}{\partial x_j} = -\frac{1}{\rho}\frac{\partial \bar{P}}{\partial x_i} + (\nu + \nu_{\mathrm{SGS}})\frac{\partial \bar{s}_{ij}}{\partial x_j}, \tag{1}$$

$$\frac{\partial \bar{u}_i}{\partial x_i} = 0, \tag{2}$$

$$\nu_{\mathrm{SGS}} = (C_s \Delta)^2 \left[\tfrac{1}{2}\bar{s}_{ij}\bar{s}_{ij}\right]^{1/2} \tag{3}$$

$$\bar{s}_{ij} = \frac{\partial \bar{u}_i}{\partial x_j} + \frac{\partial \bar{u}_j}{\partial x_i}, \tag{4}$$

where $i, j = 1, 2, 3$, $\Delta = (Dx_1 Dx_2 Dx_3)^{1/3}$ and $C_s = 0.10$ for the 3D computation. For comparison, representative 2D computational results are also presented in this paper, with $i,j = 1, 2$, $\Delta = (Dx_1 Dx_2)^{1/2}$ and $C_s = 0.15$.

These equations are non-dimensionalized using the length of the front side of the rectangular cross section, L, and the inflow velocity, U_0. The time is non-dimensionalized by L/U_0 and pressure with ρU_0^2, where ρ is the mass density of the fluid.

The Reynolds number is thus defined as LU_0/ν, with ν being the fluid kinematic viscosity.

The boundary conditions on the solid walls are of no-slip and no-penetration type, i.e., all the velocity components of the flow in x_1, x_2 and x_3 directions are set to zero on the surface. Imaginary points inside the solid wall boundaries are specified with a quadratic interpolation in order to be consistent with accuracy of the numerical scheme. The inflow boundary condition is a constant uniform velocity set equal to unity in x_1 direction and zero in x_2 and x_3 directions. The upper and lower sides of the flow domain are set with a condition $\partial/\partial n = 0$. For outflow boundary, a similar free-boundary condition, $\partial/\partial n = 0$, can be used at infinity. However, since the numerical simulation must be conducted on a finite domain, a special treatment of this condition is required. In this simulation, the convective outflow boundary condition is used:

$$\frac{\partial \bar{u}_i}{\partial t} + U_0 \frac{\partial \bar{u}_i}{\partial x_1} = 0, \quad i = 1,2,3. \tag{5}$$

Simulation results confirm this boundary condition to be both stable and accurate for a Reynolds number of 10^5.

In this simulation, the computational domain is discretized with a staggered grid, as the Maker And Cell (MAC) method [4]. In studies involving a subgrid-scale turbulence viscosity model, it is important that the accuracy order of the finite difference scheme be high enough to ensure that the numerical diffusion caused by the discretization does not dwarf the turbulence viscosity. Such being the case, a third-order upwind difference scheme for the convection terms, in conjunction with the Leith-type scheme for the temporal marching, is applied [5–7]. The discretization algorithm has been integrated with the LES model so that the characteristics of high Reynolds number flows are captured.

To study the effect of different schemes for the convection terms in the Navier–Stokes equations, here two schemes are used, namely, the central difference and the QUICK schemes [5]. These two schemes can be expressed in one equation,

$$\frac{\partial \phi}{\partial x} \simeq \frac{1}{Dx}\left\{\left[\frac{1}{2}(\phi_i + \phi_{i+1}) - \frac{q}{8}(\phi_{i-1} - 2\phi_i + \phi_{i+1})\right] - \left[\frac{1}{2}(\phi_{i-1} + \phi_i) - \frac{q}{8}(\phi_{i-2} - 2\phi_{i-1} + \phi_i)\right]\right\}, \tag{6}$$

where, $q = 1$ corresponds to the QUICK scheme, and $q = 0$ corresponds to the central difference. Detailed derivations of the scheme are omitted for brevity. Interested readers are referred to Ref. [7]. The discretized 3D equation is given by

$$\begin{aligned}\phi_P^{N+1} = \phi_P^N + \{ & - C_e[\tfrac{1}{2}(\phi_P + \phi_E) - \tfrac{1}{2}C_e(\phi_E - \phi_P) \\ & - (\tfrac{1}{8}q + \tfrac{1}{24} - \gamma_1 - \tfrac{1}{6}C_{e^2})(\phi_E - 2\phi_P + \phi_W)] \\ & + C_w[\tfrac{1}{2}(\phi_P + \phi_W) - \tfrac{1}{2}C_W(\phi_P - \phi_W)\end{aligned}$$

$$
\begin{aligned}
&- (\tfrac{1}{8}q + \tfrac{1}{24} - \gamma_1 - \tfrac{1}{6}C_w^2)(\phi_{WW} - 2\phi_W + \phi_P)] \\
&- C_n[\tfrac{1}{2}(\phi_P + \phi_N) - \tfrac{1}{2}C_n(\phi_N - \phi_P) \\
&- (\tfrac{1}{8}q + \tfrac{1}{24} - \gamma_2 - \tfrac{1}{6}C_n^2)(\phi_N - 2\phi_P + \phi_S)] \\
&+ C_s[\tfrac{1}{2}(\phi_P + \phi_S) - \tfrac{1}{2}C_s(\phi_P - \phi_S) \\
&- (\tfrac{1}{8}q + \tfrac{1}{24} - \gamma_2 - \tfrac{1}{6}C_s^2)(\phi_P - 2\phi_S + \phi_{SS})] \\
&- C_f[\tfrac{1}{2}(\phi_P + \phi_F) - \tfrac{1}{2}C_f(\phi_F - \phi_P) \\
&- (\tfrac{1}{8}q + \tfrac{1}{24} - \gamma_3 - \tfrac{1}{6}C_f^2)(\phi_F - 2\phi_P + \phi_B)] \\
&+ C_b[\tfrac{1}{2}(\phi_P + \phi_B) - \tfrac{1}{2}C_b(\phi_P - \phi_B) \\
&- (\tfrac{1}{8}q + \tfrac{1}{24} - \gamma_3 - \tfrac{1}{6}C_b^2)(\phi_P - 2\phi_B + \phi_{BB})] \\
&+ \gamma_1(\phi_E - 2\phi_P + \phi_W) + \gamma_2(\phi_N - 2\phi_P + \phi_S) \\
&+ \gamma_3(\phi_F - 2\phi_P + \phi_B + s_p Dt\}^N, \qquad (7)
\end{aligned}
$$

where P denotes the present point, W denotes the point west (to the left) of the present point in the x_1 direction, while WW denotes the point farther to the west. Accordingly, the subscripts E (east), N (north), S (south), F (front) and B (back) may be interpreted in a similar fashion. C_e is the Courant number on the east side of the present point, i.e., $C_e = u_e Dt/Dx_1$. $\gamma_1 = (\nu + \nu_{SGS})Dt/Dx_1^2$, $\gamma_2 = (\nu + \nu_{SGS})Dt/Dx_2^2$, and $\gamma_3 = (\nu + \nu_{SGS})Dt/Dx_3^2$. Here ν_{SGS} is the subgrid-scale viscosity, calculated using Eq. (3). The pressure field is solved with a successive overrelaxation method, ensuring that the computed flow field is divergence free. The presented equations are for a uniform grid mesh, but both uniform and non-uniform grid meshes were used in the calculations.

The computational domain is $27L$ in the streamwise direction, $18L$ in the cross stream direction, and $2L$ in the spanwise direction. The prism is located at the center in the lateral direction, and its front face is at a distance of 8L from the entrance flow boundary.

The computations were carried out primarily using the computer facilities at the University of Notre Dame and at the National Center for Supercomputing Applications. A flow simulation at a Reynolds number of 10^5 required about 160 h of user time on an SGI Power Challenge computer, to march for a non-dimensional time of 100.

3. Simulation results

3.1. Velocity field

Time histories of the velocity and pressure field are generated using the method described above, with a computed potential flow for the same configuration, or the

output from a previous 2D or 3D simulation, serving as the initial flow field. In each case, the vortex shedding process (for Re = 10^5) begins without introducing any initial perturbation. When the 3D simulation is initially started from a 2D flow, it takes about a non-dimensional time of 50 to reach a fully developed 3D flow, and results reported hereafter are for the well-developed period. The statistical values (mean and RMS) are obtained over a time length of 500. Unless otherwise stated, all the reported 3D results in this paper are based on the QUICK scheme, using a grid size of $Dx = Dy = 0.05$ near the bluff body and a uniform $Dz = 0.2$ in the z-direction.

The time-averaged streamwise velocity on the symmetry line is reported in Fig. 1, together with the experimental results by Lyn [8] and Durão et al. [9], and the numerical results by Murakami and Mochida [1] and Franke and Rodi [10, 11]. Upstream of the square, the difference among the compared studies is extremely small. In the wake flow, both the current 2D and 3D simulation results show a good agreement with the experimental results. It should be noted that the three-dimensional results of Murakami and Mochida [1] deviate from the current simulation results, although both are based on LES modeling. The discrepancy may be due to the employed numerical methods and boundary conditions rather than the turbulence model itself. A similar discrepancy is also exhibited by the pressure results shown in the next subsection. Different turbulence models do influence the results, as the differences among the results obtained employing k–ε, RSE and LES are depicted in Fig. 1.

As seen in Fig. 1, the mean values from the 2D simulation are not significantly different from the 3D results, although they are obtained with far less computational

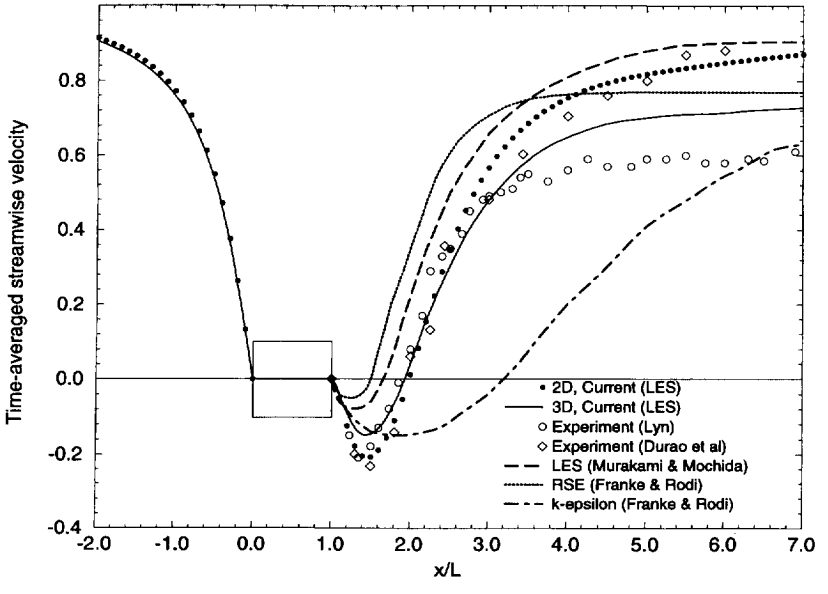

Fig. 1. Time-averaged streamwise velocity.

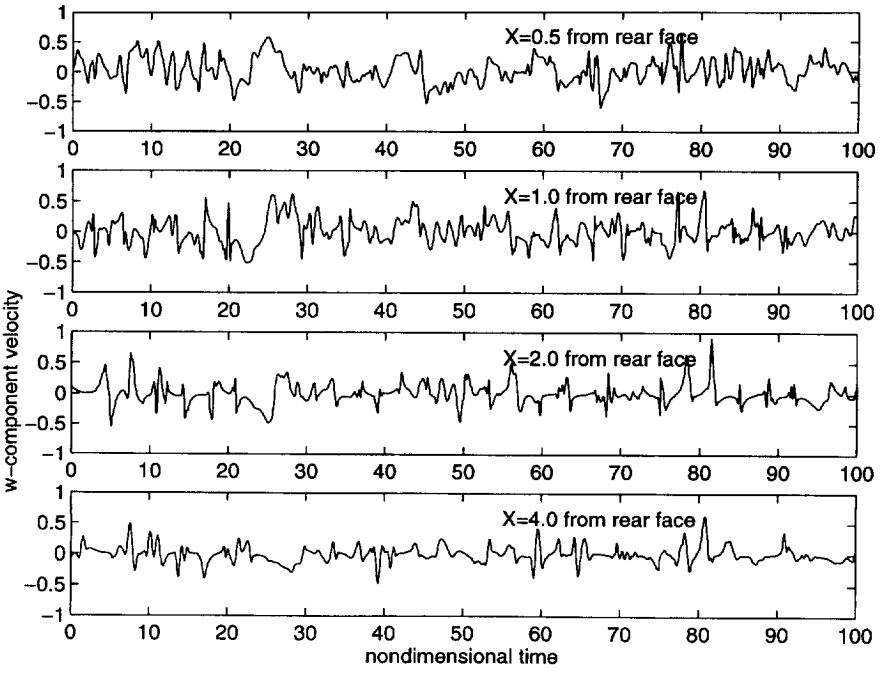

Fig. 2. Time history of w-component velocity in the wake.

effort. Nevertheless, in the 3D simulation, the spanwise component of velocity is present, and it does redistribute energy from the x–y plane. Fig. 2 shows the time history of the spanwise velocity component at four downstream locations in the wake on the centerline, distance of $0.5L$, $1.0L$, $2.0L$ and $4.0L$ from the rear face of the prism, respectively.

3.2. *Pressure field*

3.2.1. *Mean Pressure distribution on surface of prism*

In Fig. 3, the distribution of the mean pressure coefficient, defined as $\bar{p}/(\frac{1}{2}\rho U_0^2)$, on the surface of a square prism, is compared with the experimental data and the numerical results of Murakami and Mochida [1]. The current 2D and 3D simulation results are generally close to one another and both compare well with the experimental data, except at two points at the front corners on the side faces. It needs to be emphasized that the grid size of the 3D simulation is $Dx = Dy = 0.05$ near the body while it is $Dx = Dy = 0.1$ for the 2D case. The 2D results of Murakami and Mochida [1] are very different from their 3D simulation and the experimental results. The team's 3D results still exhibit a significant deviation from the experimental data in the regions of negative pressure. This is especially evident in the 3D results for the leeward face, which show the pressure coefficient to be around -1.02, as compared to the

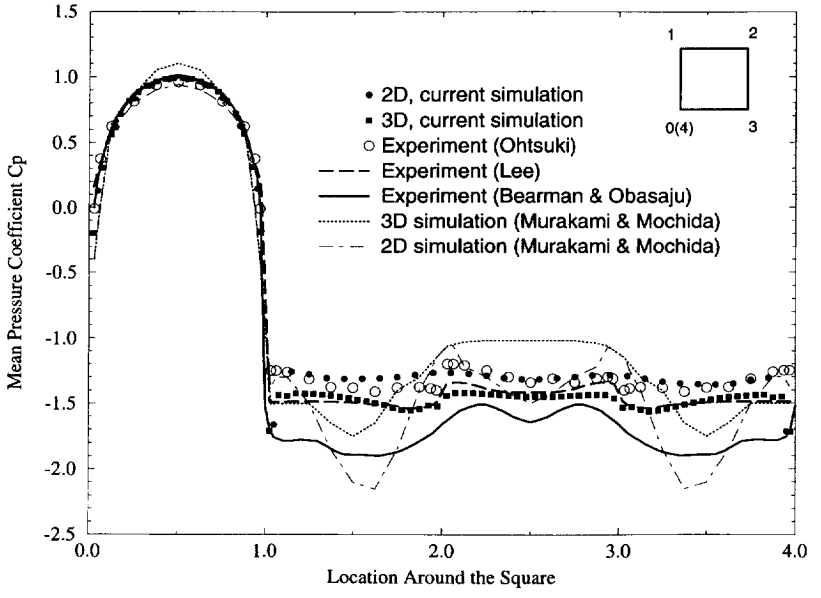

Fig. 3. Distribution of the mean pressure coefficient. Experimental values from Refs. [12–14] and simulations from Ref. [1].

experimental value of near $-1.3-\ -1.5$. As mentioned earlier concerning the results for the centerline velocity, the discrepancies between the current simulation and the results by Murakami and Mochida [1] may not be due to the turbulence model, since both used LES, but may instead be a result of the numerical method or boundary condition specifications. For example, the treatment of the outflow boundary by a free boundary condition ($\partial/\partial n = 0$) may introduce errors in the simulated results. As noted earlier, a convective boundary condition is more realistic.

3.2.2. RMS pressure distribution on surface of prism

In Fig. 4, RMS values of the pressure fluctuations on the surface of a square prism are presented. The lowest RMS is at the center of the front surface, while higher values of pressure fluctuations appear on the two side faces. On the rear side, the fluctuations decrease as the center line on the back face is approached. Again, numerical results are compared with the available experimental results and are found to be in a good agreement. The range of Reynolds numbers in the cited references in Fig. 4 are: Bearman and Obasaju [13] ($Re = 2 \times 10^4$), Lee [14] ($Re = 1.76 \times 10^5$), and Wilkinson [15] ($Re = 10^4$–10^5). Note that the 3D results of Murakami and Mochida [1] are also very close to the experimental results, while their 2D results differ substantially.

3.2.3. Integral quantities

Table 1 lists the integral quantities and their comparison with the experimental results. The 2D and 3D results (with near-body grid size of $\frac{1}{20}$) are close to one another

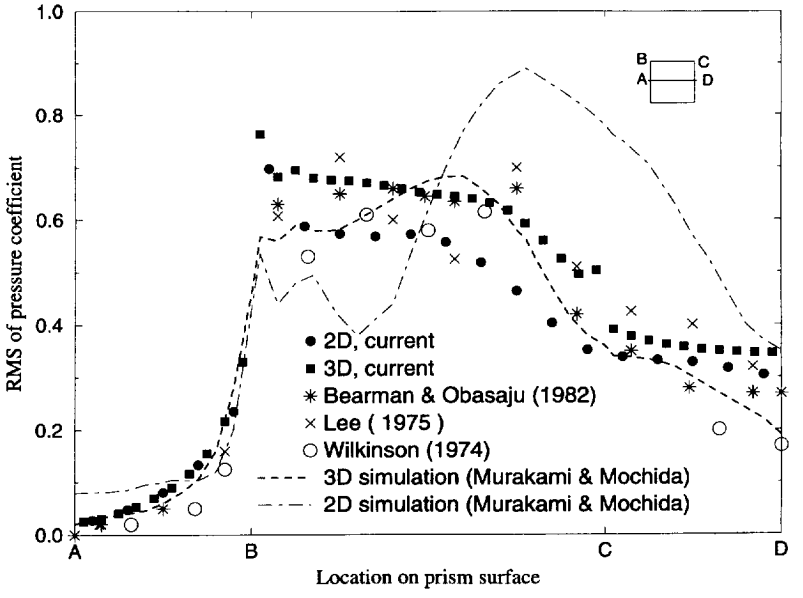

Fig. 4. Distribution of the RMS pressure.

Table 1
Comparison of mean and RMS of C_L and C_D and Strouhal number with experiments

	RMS of C_L	Mean of C_D	RMS of C_D	St. Number
2D, $Dx,Dy = \frac{1}{10}$	1.06	2.01	0.21	0.14
3D, $Dx,Dy = \frac{1}{20}$	1.15	2.14	0.25	0.135
3D, $Dx,Dy = \frac{1}{15}$	1.07	2.19	0.12	0.138
3D, $Dx,Dy = \frac{1}{10}$	0.33	1.78	0.06	0.149
Vickery, 1 [16]	1.32		0.17	0.12
Vickery, 2 [16]	1.27		0.17	
Lee [14]	1.22	2.05	0.22	
Bearman and Obasaju [13]	1.2			0.13
Nakamura and Mizota [17]	1.0			
Okajima (1982) [18]				0.13

and both agree well with experimental findings. At the same time, it is found that 3D results with course grid size ($Dx = Dy = \frac{1}{10}$) give much lower RMS values of both the lift coefficient C_L and the drag coefficient C_D. The results with the grid size of ($Dx = Dy = \frac{1}{15}$) are closer, while the results with the grid size of ($Dx = Dy = \frac{1}{20}$) are the closest to the experimental values. The Strouhal number from simulations with different grid sizes exhibits a similar trend.

3.2.4. Correlation of pressure fluctuations

Fig. 5 shows the correlation coefficients of pressure fluctuations on the surface of the prism with reference to a point marked on the upper side face. Both the 2D and 3D results are plotted and compared with the experimental findings by Lee [14]. The results indicate a dominant presence of an antisymmetric correlation pattern associated with vortex shedding, and the numerical results are in very good agreement with experimental data. From Figs. 1, 3–5 and Table 1, it may be observed that the 2D and 3D results are not far apart suggesting dominance of 2D structure in the vortical flow field. This is in contrast with earlier reports by other investigators (e.g., Ref. [1]).

3.3. Grid refinement study

To study the accuracy of the numerical scheme and the resolution requirement for the specific flow simulated, a grid refinement study is conducted. Roache [19] suggested a method for reporting numerical convergence uniformly, based on Richardson extrapolation. For the LES, there has been limited experience about reporting of errors associated with grid refinement. One way to refine the grids for an LES is to keep the value of Δ in the Smagorinsky model (Eq. (3)) invariant, while refining Dx, Dy and Dz. The other approach involves refinement of grid uniformly, while allowing Δ vary in each refinement since Δ is defined as $(DxDyDz)^{1/3}$ in the Smagorinsky model. Theoretically, the results should converge to the "true solution" as the grid is refined.

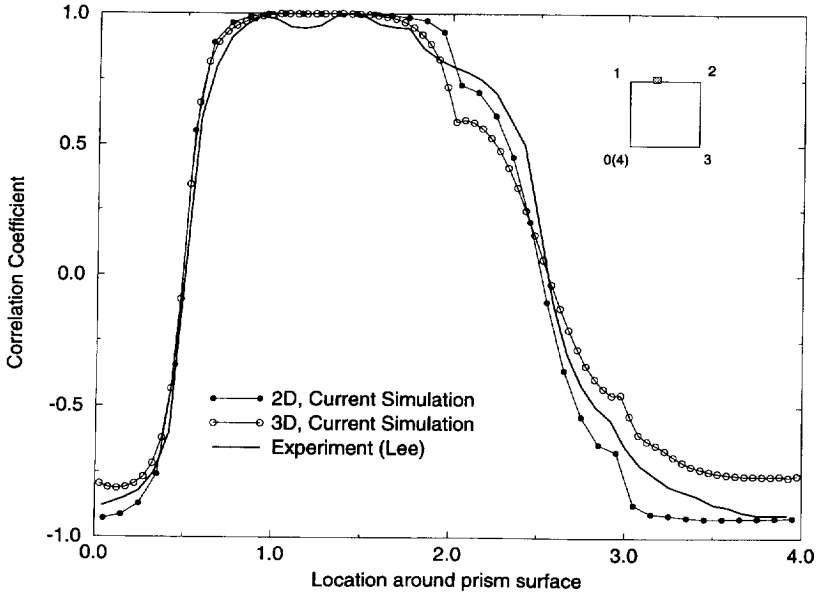

Fig. 5. Chordwise correlation of pressure.

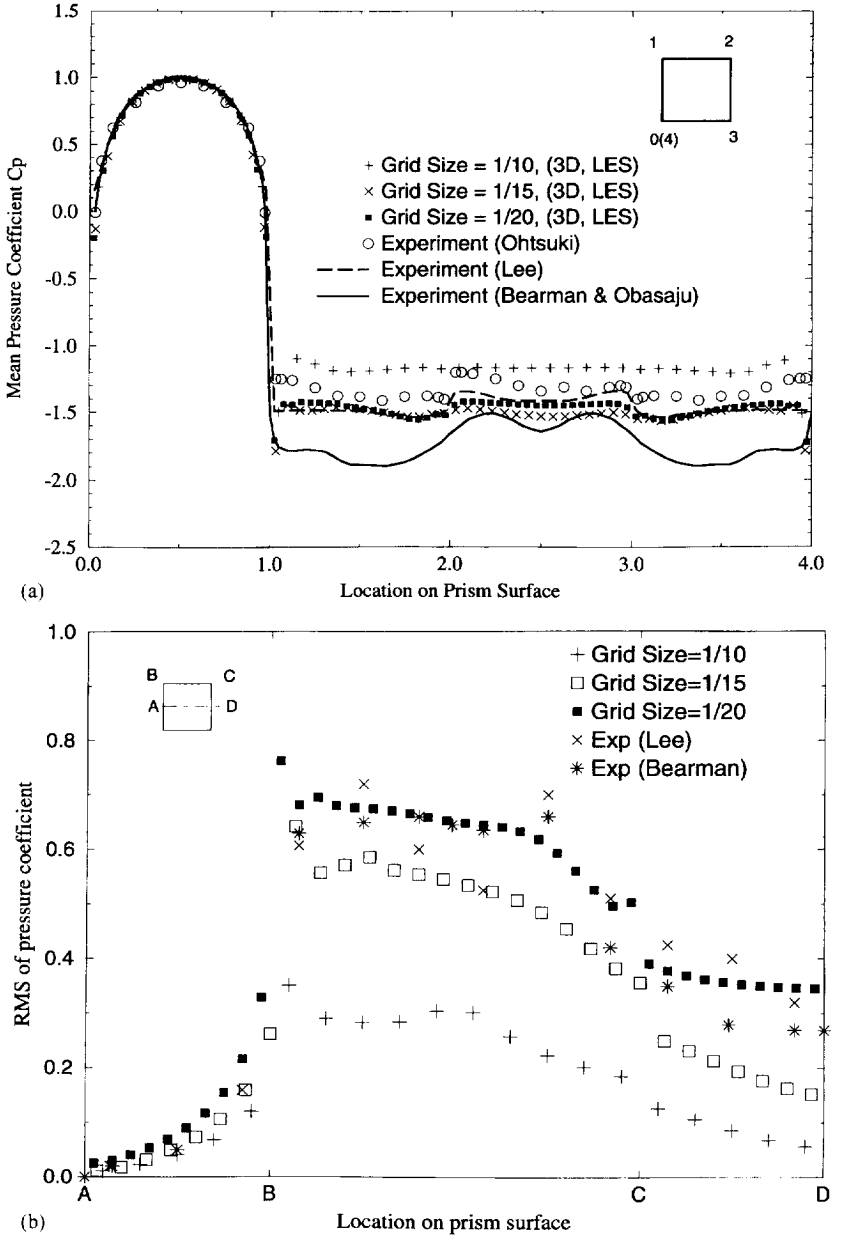

Fig. 6. Comparison of results with different grid sizes: (a) mean pressure; (b) RMS pressure.

These two approaches are not equivalent and may not produce the same results, thus warranting additional investigation through numerical experiments.

In this study, several grid sizes are used, including both uniform and variable-size grids. Δ is also varied as $(DxDyDz)^{1/3}$. For the uniform meshes, three grid sizes are tested, i.e., $Dx = Dy = \frac{1}{10}$ $Dx = Dy = \frac{1}{12}$ (not reported here) and $Dx = Dy = \frac{1}{15}$. To save computational effort, a mesh with variable grid size was used for the case with the near-body grid sizes of $Dx_{\text{body}} = Dy_{\text{body}} = \frac{1}{20}$. For all these cases, the same grid size was used in the spanwise direction, $Dz = 0.2$. The results concerning the mean and RMS pressure distribution on the body surface are presented in Fig. 6, which again confirms the importance of grid resolution. Course grids result in a much lower level of RMS pressure fluctuation, and a higher (less negative) base pressure, which are similar to a flow with excessive dissipation. These deviations cannot be corrected by modifying the C_s value in the SGS model (Eq. (3)), varying the time step Dt, or using a different scheme (QUICK or central difference) for the discretization of the convection terms. There is a clear trend demonstrating that simulations approach realistic values as the grids are refined, with the most refined grids ($Dx_{\text{body}} = Dy_{\text{body}} = \frac{1}{20}$) leading to the closest agreement with the experimental values.

3.4. Comparison of central difference and QUICK schemes

The QUICK and the central difference schemes are used to discretize the convection terms, and the obtained simulation results (with grid size of $Dx_{\text{body}} = Dy_{\text{body}} = \frac{1}{20}$) are compared in Fig. 7. Only insignificant differences are observed and both results are close to experimental data, which indicates the insignificance, at the employed grid resolution, of numerical dissipation in the QUICK scheme due to its upwind-biased nature. The leading order error of the QUICK scheme is proportional to the third power of grid size and the fourth-order derivative of velocity. Thus, the QUICK scheme is slightly dissipative, but does not contain numerical viscosity (if numerical viscosity is defined as error proportional to the second-order derivative of velocity).

3.5. Effect of time step

In a direct numerical simulation of turbulent channel flow, Choi and Moin [20] reported that computational time steps substantially influence the statistical results. In their study, for large time steps ($Dt^+ = 1.6$ and 2, corresponding to CFL = 4 and 5) near or larger than the Kolmogorov time scale (2.4), the simulations resulted in a laminar flow instead of turbulent. Up to now, the authors are not aware of such reports concerning large eddy simulations, and computations are conducted here with two different time steps ($Dt = 0.0125$ and 0.00625, corresponding to CFL = 0.25 and 0.125) to study this effect. Results concerning pressure are reflected in Fig. 7, from which it can be seen that the effect of different Dt are noticeable but not significant. This suggests that a time step of $Dt = 0.0125$ is refined enough to resolve the flow satisfactorily.

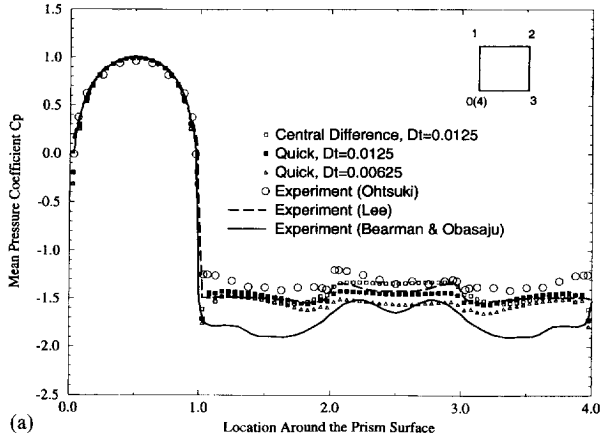

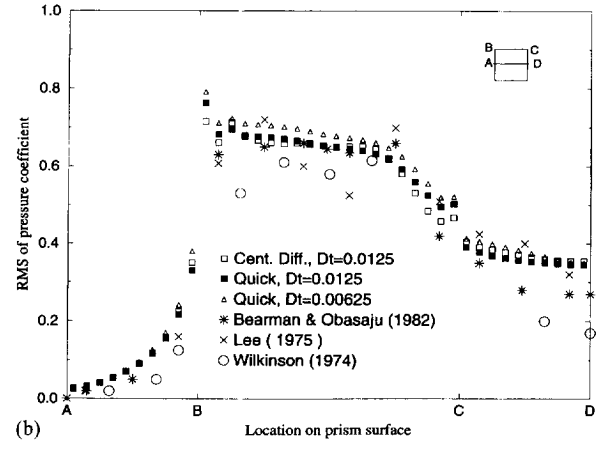

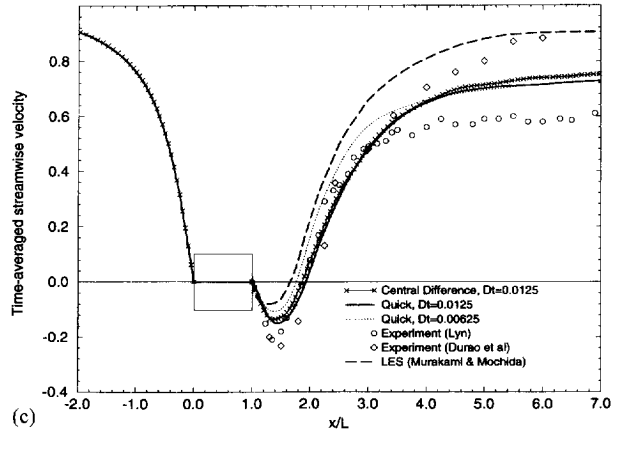

Fig. 7. Comparison of results based on central difference and QUICK methods, and different time steps: (a) mean pressure; (b) RMS pressure; and (c) time-averaged streamwise velocity.

4. Conclusions

Using QUICK and central difference schemes for the convection terms, the Leith method for temporal marching and the Smagorinsky model for subgrid-scale viscosity, 3D numerical algorithm based on a staggered grid gives results in a very good agreement with the available experimental data. A grid refinement study reveals that sufficient resolution is very important in 3D LES simulations. An insufficient resolution leads to much lower RMS values of pressure fluctuations. A comparison of third-order QUICK and central difference schemes for the discretization of the convection terms shows only minor differences, and suggests relative insignificance of the numerical dissipation introduced by the upwind nature of QUICK, as long as the grid resolution is sufficient. The influence of time step is also investigated, and small effects are found for the two tested Dt values ($Dt = 0.0125$ and 0.00625, corresponding to CFL = 0.25 and 0.125).

Acknowledgements

This study was partially supported by NCSA Grant No. BCS960002N, ONR Grant No. 00014-93-1-0761 and NSF Grant No. CMS-9503779.

References

[1] S. Murakami, A. Mochida, On turbulent vortex shedding flow past 2D square cylinder predicted by CFD, J. Wind Eng. Ind. Aerodyn. 54/55 (1995) 191–211.
[2] T. Tamura, Accuracy of the very large computation for aerodynamic forces acting on a stationary or an oscillating cylinder-type structure, IWEF Workshop on CFD for Prediction of Wind Loading on Building and Structures, 9 September, 1995, Tokyo Institute of Technology (Nagatsuta Campus), Yokohama, Japan, pp. 2.1–2.22.
[3] W. Rodi, J.H. Ferziger, M. Breuer, M. Pourquié, 1996, Status of Large Eddy Simulation: Results of a Workshop, personal communication, pp. 1–35.
[4] F.H. Harlow, J.E. Welch, Numerical calculation of time-dependent viscous incompressible flow of fluid with free surface, Phys. Fluids 8 (1965) 2182–2189.
[5] B.P. Leonard, A stable and accurate convective modelling procedure based on quadratic upstream interpolation, Comput. Methods App. Mech. Eng. 19 (1979) 59–98.
[6] R.W. Davis, E.F. Moore, A numerical study of vortex shedding from rectangles, J. Fluid Mech. 116 (1982) 475–506.
[7] D. Yu, A. Kareem, Numerical Simulation of Pressure Field Around Two-Dimensional Rectangular Prism, Technical Report No. NDCE-96-002, Department of Civil Engineering and Geological Sciences, University of Notre Dame, 1996.
[8] D.A. Lyn, Phase-averaged turbulence measurements in the separated shear flow around square cylinder, in: Proc. 23rd Cong. Int. Ass. Hydraulic Research, Ottawa, Canada, 21–25 August 1989, pp. A85–A92.
[9] D.F.G. Durão, M.V. Heitor, J.C.F. Pereira, Measurements of turbulent and periodic flows around a square cross-section cylinder, Exp. Fluids 6 (1988) 298–304.
[10] R. Franke, W. Rodi, Calculation of vortex shedding past a square cylinder with various turbulence models, in: Proc. of the 8th Symp. on Turbulent Shear Flows, Munich, Germany, 1991, p. 189.

[11] W. Rodi, On the simulation of turbulent flow past bluff bodies, J. Wind Eng. Ind. Aerodyn. 46/47 (1993) 3–19.
[12] Y. Ohtsuki, Wind tunnel experiments on aerodynamic forces and pressure distributions of rectangular cylinders in a uniform flow, Proc. 5th Symp. on Wind Effects on Structures, Tokyo, Japan, 1976, pp. 169–175.
[13] P.W. Bearman, E.D. Obasaju, An experimental study of pressure fluctuations on fixed and oscillation square-section cylinders, J. Fluid Mech. 119 (1982) 297–321.
[14] B.E. Lee, The effect of turbulence on the surface pressure field of a square prism, J. Fluid Mech. 69 (1975) 263–282.
[15] R.H. Wilkinson, On the vortex-induced loading on long bluff cylinders. Ph.D. Thesis, Faculty of Engineering, University of Bristol, England, 1974.
[16] B.J. Vickery, Fluctuating lift and drag on a long cylinder of square cross-section in a smooth and in a turbulent stream, J. Fluid Mech. 125 (1966) 481–494.
[17] Y. Nakamura, T. Mizota, Unsteady lifts and wakes of oscillating rectangular prisms, Proc. A.S.C.E.: J. Eng. Mech. Div. 101 (EM6) (1975) 855–871.
[18] A. Okajima, Strouhal numbers of rectangular cylinders, J. Fluid Mech. 123 (1982) 379–398.
[19] P.J. Roache, Perspective: a method for uniform reporting of grid refinement studies, J. Fluids Eng. 116 (1994) 405–413.
[20] H. Choi, P. Moin, Effects of the computational time step on numerical solutions of turbulent flow, J. Comput. Phys. 113 (1994) 1–4.